12-1-2012

The Effect of Cone Opsin Mutations on Retinal Structure and the Integrity of the Photoreceptor Mosaic

Joseph Carroll
Marquette University

Alfredo Dubra
Marquette University

Jessica C. Gardner
UCL Institute of Ophthalmology

Liliana Mizrahi-Meissonnier
Hadassah-Hebrew University Medical Center

Robert F. Cooper
Marquette University

See next page for additional authors

Accepted version. *Investigative Ophthalmology & Visual Science*, Vol. 53, No. 13 (December 2012): 8006-8015. DOI.

Authors
Joseph Carroll, Alfredo Dubra, Jessica C. Gardner, Liliana Mizrahi-Meissonnier, Robert F. Cooper, Adam M. Dubis, Rick Nordgren, Mohamed Genead, Thomas B. Connor Jr., Kimberly E. Stepien, Dror Sharon, David M. Hunt, Eyal Banin, Alison J. Hardcastle, Anthony T. Moore, David R. Williams, Gerald Fishman, Jay Neitz, Maureen Neitz, and Michel Michaelides

The Effect of Cone Opsin Mutations on Retinal Structure and the Integrity of the Photoreceptor Mosaic

Joseph Carroll
Department of Ophthalmology
Department of Cell Biology, Neurobiology, and Anatomy
Medical College of Wisconsin
Milwaukee, WI
Alfredo Dubra
Department of Ophthalmology
Department of Biophysics, Medical College of Wisconsin,
Milwaukee, WI
Flaum Eye Institute and
Center for Visual Science, University of Rochester
Rochester, NY
Jessica C. Gardner
UCL Institute of Ophthalmology
London, United Kingdom
Liliana Mizrahi-Meissonnier
Department of Ophthalmology
Hadassah-Hebrew University Medical Center
Jerusalem, Israel

Investigative Ophthalmology and Visual Science, Vol. 53, No. 13 (December 2012): pg. 8006-8015. DOI.

Robert F. Cooper
Department of Biomedical Engineering, Marquette University
Milwaukee, WI
Adam M. Dubis
Department of Cell Biology, Neurobiology, and Anatomy
Medical College of Wisconsin
Milwaukee, WI
Rick Nordgren
Department of Ophthalmology, Medical College of Wisconsin,
Milwaukee, WI
Mohamed Genead
Chicago Lighthouse for People Who Are Blind or Visually Impaired, Department of Ophthalmology and Visual Sciences, University of Illinois-Chicago
Chicago, IL
Thomas B. Connor, Jr.
Departments of Ophthalmology, Medical College of Wisconsin,
Milwaukee, WI
Kimberly E. Stepien
Departments of Ophthalmology, Medical College of Wisconsin,
Milwaukee, WI
Dror Sharon
Department of Ophthalmology, Hadassah-Hebrew University Medical Center
Jerusalem, Israel
David M. Hunt
UCL Institute of Ophthalmology
London, United Kingdom
School of Animal Biology and Lions Eye Institute
University of Western Australia
Perth, Australia

Investigative Ophthalmology and Visual Science, Vol. 53, No. 13 (December 2012): pg. 8006-8015. DOI.

Eyal Banin
Department of Ophthalmology, Hadassah-Hebrew University Medical Center
Jerusalem, Israel
Alison J. Hardcastle
UCL Institute of Ophthalmology
London, United Kingdom
Anthony T. Moore
UCL Institute of Ophthalmology
Moorfields Eye Hospital
London, United Kingdom
David R. Williams
Flaum Eye Institute
Center for Visual Science, University of Rochester
Rochester, NY
Gerald Fishman
Chicago Lighthouse for People Who Are Blind or Visually Impaired
Department of Ophthalmology and Visual Sciences
University of Illinois-Chicago
Chicago, IL
Jay Neitz
Department of Ophthalmology, University of Washington
Seattle, WA
Maureen Neitz
Department of Ophthalmology, University of Washington
Seattle, WA
Michel Michaelides
UCL Institute of Ophthalmology
Moorfields Eye Hospital
London, United Kingdom

Investigative Ophthalmology and Visual Science, Vol. 53, No. 13 (December 2012): pg. 8006-8015. DOI.

Abstract

Purpose.

To evaluate retinal structure and photoreceptor mosaic integrity in subjects with *OPN1LW* and *OPN1MW* mutations.

Methods.

Eleven subjects were recruited, eight of whom have been previously described. Cone and rod density was measured using images of the photoreceptor mosaic obtained from an adaptive optics scanning light ophthalmoscope (AOSLO). Total retinal thickness, inner retinal thickness, and outer nuclear layer plus Henle fiber layer (ONL+HFL) thickness were measured using cross-sectional spectral-domain optical coherence tomography (SD-OCT) images. Molecular genetic analyses were performed to characterize the *OPN1LW*/*OPN1MW* gene array.

Results.

While disruptions in retinal lamination and cone mosaic structure were observed in all subjects, genotype-specific differences were also observed. For example, subjects with "L/M interchange" mutations resulting from intermixing of ancestral *OPN1LW* and *OPN1MW* genes had significant residual cone structure in the parafovea (~25% of normal), despite widespread retinal disruption that included a large foveal lesion and thinning of the parafoveal inner retina. These subjects also reported a later-onset, progressive loss of visual function. In contrast, subjects with the C203R missense mutation presented with congenital blue cone monochromacy, with retinal lamination defects being restricted to the ONL+HFL and the degree of residual cone structure (8% of normal) being consistent with that expected for the S-cone submosaic.

Conclusions.

The photoreceptor phenotype associated with *OPN1LW* and *OPN1MW* mutations is highly variable. These findings have implications

Investigative Ophthalmology and Visual Science, Vol. 53, No. 13 (December 2012): pg. 8006-8015. DOI.

for the potential restoration of visual function in subjects with opsin mutations. Our study highlights the importance of high-resolution phenotyping to characterize cellular structure in inherited retinal disease; such information will be critical for selecting patients most likely to respond to therapeutic intervention and for establishing a baseline for evaluating treatment efficacy.

Introduction

Mutations in the long-wavelength (L) and middle-wavelength (M) cone opsin genes (designated *OPN1LW* and *OPN1MW*, respectively) have been associated with a wide range of visual defects including red-green color vision deficiency, blue cone monochromacy (BCM), X-linked cone dystrophy, X-linked cone dysfunction, and high myopia with abnormal cone function.[1–16] While characterization of visual function in these individuals is relatively straightforward, less is known about how the presence of *OPN1LW* and *OPN1MW* mutations affects retinal structure. Such information will be of paramount importance for advancing efforts to restore cone function in individuals with *OPN1LW* and *OPN1MW* mutations.

Recent studies have shown that *OPN1LW* and *OPN1MW* mutations resulting in congenital red-green color vision defects are associated with a variable retinal phenotype, with some individuals showing disrupted cone structure and/or thinning of the outer nuclear layer (ONL).[8,14,17,18] It is difficult to draw definite conclusions about the pathogenicity of a specific mutant from comparisons of these individuals, as there may be other factors influencing the retinal phenotype. For example, during development, there is competition between the first two genes in the X-chromosome opsin array in the nascent L/M cones that ends with only one of the two genes being expressed in each cell.[19] It has been shown that the relative proportion of cones expressing each of the two genes in the L/M array varies widely (over 40-fold).[20,21] Thus previously observed differences in retinal phenotype may be confounded by differences in the relative expression of the mutant opsin with respect to the normal opsin. As the degree of retained cone photoreceptor structure is related to the

Investigative Ophthalmology and Visual Science, Vol. 53, No. 13 (December 2012): pg. 8006-8015. DOI.

therapeutic potential of a given retina,[22] elucidation of genotype-specific retinal phenotypes is essential.

In one of the more serious vision disorders associated with *OPN1LW* and *OPN1MW* mutations, a single type of mutant opsin is expressed in all the cones that would have been L or M in a normal eye. In these subjects, rods and short-wavelength (S) cones are the only photoreceptors expressing normal photopigments. These individuals offer the opportunity to directly evaluate the effect of different *OPN1LW* and *OPN1MW* mutations. These mutations can be placed into one of three categories: (1) mutations that produced random nonhomologous missense substitutions at single amino acid positions[1,3,12,16]; (2) partial or complete deletion of an exon[15,23]; and (3) a recently identified category involving intermixing of ancestral *OPN1LW* and *OPN1MW* genes to produce "L/M interchange" mutations with deleterious combinations of nucleotides at normal polymorphic positions.[7,8,10,13] While at least one L/M interchange mutation has been shown to directly cause cone malfunction (Greenwald SH, et al. *IOVS* 2012;53:ARVO E-Abstract 4643), it was recently shown that in addition to any functional changes in the photopigment caused by the mutations, many of the L/M interchange mutations also interfere with recognition of exon 3 by the splicing mechanism.[24] Some of the variants incompletely interfere with splicing, so full-length mRNA is produced as well as the inappropriately spliced transcript. Whether there are structural differences between the mutation categories, or for different mutations within a category, has been unknown.

Here we used adaptive optics scanning laser ophthalmoscopy (AOSLO) and spectral-domain optical coherence tomography (SD-OCT) to examine 11 subjects for whom all cones except the S cones express one of six mutant opsins. There were differences in the anatomy and in the course and severity of vision loss across mutation categories. The subjects with L/M interchange mutations reported a later-onset progressive loss of visual function, while those with the C203R mutation showed a typical congenital BCM phenotype. We observed significant disruption of retinal lamination and of cone mosaic topography in all subjects, though the degree of disruption was generally greater for subjects with L/M interchange mutations than for

Investigative Ophthalmology and Visual Science, Vol. 53, No. 13 (December 2012): pg. 8006-8015. DOI.

those with random mutations. These differences provide insight into the underlying mechanisms responsible for loss of structure and function in these subjects. Furthermore, while the cone loss observed may limit success of any efforts to restore L/M cone function using gene therapy in any of these subjects, it may be possible to develop strategies to slow or halt the degenerative changes in people harboring L/M interchange mutations.

Methods

Human Subjects

Written informed consent was obtained after the nature and possible consequences of the study were explained. This study followed the tenets of the Declaration of Helsinki and was approved by all local ethics committees. We examined eight subjects for whom the clinical phenotype has been previously described and three new subjects (see Table and Supplementary Material, http://www.iovs.org/content/53/13/8006/suppl/DC1). Two male subjects (JC_0826, 22 years; JC_0847, 23 years) with normal color vision were included for comparison, and data from two previously published normative databases were used for comparison of the SD-OCT studies. The data used for comparison against the horizontal line scans consisted of 93 subjects with an average age of 25.7 ± 8.2 years,[14] and the data used for comparison against the topographical thickness maps consisted of 60 subjects with an average age of 29 ± 8.42 years.[25] Axial length measurements were obtained on all subjects (Zeiss IOL Master; Carl Zeiss Meditec, Dublin, CA) in order to determine the scale (in microns per pixel) of each retinal image. Prior to all retinal imaging, each eye was dilated and cycloplegia was induced through topical application of a combination of phenylephrine hydrochloride (2.5%) and tropicamide (1%).

Investigative Ophthalmology and Visual Science, Vol. 53, No. 13 (December 2012): pg. 8006-8015. DOI.

Subject	Age, y	Axial Length, mm (OD, OS)	BCVA (OD, OS)	L/M Array Structure	L/M Mutation	Source*
JC_0183	16	25.65, 25.92	20/80, 20/80	0L, 1M	C203R†	Fam. C, V:4[12]
JC_0184	13	24.85, 24.76	20/120, 20/120	0L, 1M	C203R†	Fam. C, V:5[12]
JC_0440	18	25.49, 25.75	20/80, 20/80	0L, 2M	C203R† ‡	Fam. 1, 2.1[15]
JC_0441	18	25.21, 25.12	20/80, 20/80	0L, 2M	C203R† ‡	Fam. 1, 2.2[15]
JC_0355	31	24.54, 24.59	20/80, 20/125	1L, 1M	W177R§ ‡	IV:1[16]
JC_0356	30	25.90, 25.88	20/125, 20/125	1L, 1M	W177R§ ‡	IV:2[16]
JC_0347	32	24.77, 24.25	20/125, 20/125	1L, 0M	LVAVA‖	This study
JC_0564	45	27.08, 26.58	20/100, 20/100	0L, 1M	LVAVA‖	This study
JC_0118	32	25.83, 26.43	20/40, 20/40	1L, 0M	LIAVS‖	MOL0250 III:2[13]
KS_0577	38	23.71, 23.93	20/70, 20/100	0L, 1M	LVVVA‖	This study
JC_0430	26	25.40, 25.31	20/120, 20/120	0L, 1M	Exon 2 deletion	Fam. A, III:3[12]

Table. Clinical and Genetic Summary

Fam., Family.

* Previous report of genotype and/or phenotype.

† Substitution of cysteine (C) for arginine (R) at position 203.

‡ Both genes in the array encode mutation.

§ Substitution of tryptophan (W) for arginine at position 177.

‖ Sequence of polymorphic amino acids encoded by exon 3 of the L/M gene present in the subjects' L/M gene array (153, 171, 174, 178, 180). L, leucine; I, isoleucine; A, alanine; V, valine; S, serine.

Molecular Genetics

For the three newly recruited subjects, DNA was isolated from whole blood, and the opsin genes were amplified and sequenced using previously described methods.[7]

Investigative Ophthalmology and Visual Science, Vol. 53, No. 13 (December 2012): pg. 8006-8015. DOI.

Spectral-Domain Optical Coherence Tomography

Volumetric images of the macula were obtained using high-definition OCT (Cirrus HD-OCT; Carl Zeiss Meditec). Volumes were nominally 6 mm × 6 mm and consisted of 128 B-scans (512 A-scans/B-scan). Retinal thickness was calculated using the Macular Analysis software on the Cirrus (software version 5.0; Carl Zeiss Meditec), which is automatically determined via measurement of the difference between the inner limiting membrane (ILM) and retinal pigment epithelium (RPE) boundaries. High-resolution SD-OCT images of the macula were acquired (Bioptigen, Research Triangle Park, NC). High-density line scans (1000 A-scans/B-scan, 100 repeated B-scans) were acquired through the foveal center, then registered and averaged as previously described.[26] No transformation (e.g., flattening), filtering, or other postprocessing was applied to these images.

For retinal sublayer analysis, we manually segmented the ILM, the outer plexiform layer (OPL), the external limiting membrane (ELM), and the RPE on the high-resolution line scans as previously described using ImageJ (National Institute of Mental Health, Bethesda, MD).[14] The ILM–RPE distance provides total retinal thickness, the ILM–OPL distance provides the inner retinal thickness, and the OPL–ELM distance provides the ONL plus Henle fiber layer thickness (ONL+HFL).

Adaptive Optics Retinal Imaging

An adaptive optics scanning light ophthalmoscope (AOSLO) was used to obtain images of the photoreceptor mosaic at various retinal locations. JC_0183, JC_0184, JC_0440, JC_0441, JC_0355, JC_0356, JC_0118, and JC_0430 were imaged at the University of Rochester; details of this imaging system have been previously published.[27] The remaining three subjects and the normal controls were imaged at the Medical College of Wisconsin, and details of this system have also been published.[28] The systems derive from the basic design described by Gray et al.,[29] with the afocal telescopes folded to varying degrees.[27] Both systems utilized a 97-channel deformable mirror (ALPAO, Biviers, France) as the wavefront corrector, with a Shack-Hartman wavefront sensor used to measure the wavefront. The imaging source was either

Investigative Ophthalmology and Visual Science, Vol. 53, No. 13 (December 2012): pg. 8006-8015. DOI.

a 775 nm or a 796 nm super-luminescent diode (Inphenix Inc., Livermore, CA), and the light exposure was kept below the safe maximum permissible exposure set forth by ANSI.[30,31] Images were processed to remove distortions induced by the sinusoidal motion of the resonant scanner by estimating the distortion from images of a calibrated Ronchi ruling and then resampling the images over a grid of equally spaced pixels. A separate calibration was done for each subject. Images were registered to improve signal-to-noise as previously described.[32]

The registered images from each subject were combined into a single montage (Adobe Photoshop; Adobe Systems, Inc., San Jose, CA). This montage was scaled and aligned to the LSO image from the HD-OCT, in which a crosshair was placed at the center of the foveal pit. The scaling was based on theoretical magnification of each system and the alignment performed using blood vessel patterns. The locations to be analyzed were determined based on the distance from the center of the foveal pit, and the original image comprising that portion of the montage was set aside for subsequent density analyses. Cone density was measured at selected retinal locations (0.4, 0.8, 1.2, 1.6, 2.0 mm) using manual identification of cone structures (80 μm × 80 μm sampling window). For rod analysis, we utilized a smaller sampling window (55 μm × 55 μm) than we did for the cone density analysis, as the cones in these subjects were more sparse and irregularly spaced. Rod density was calculated at various locations between 0.5 and 3 mm using a previously described semiautomated algorithm in which the user could add/subtract missed or erroneous cell identifications.[33]

Results

Different Genotype Classes Associated with Distinct Clinical Phenotypes

The Table provides a summary of subject demographics, with the clinical phenotype on 8 of the 11 having been reported previously. All four subjects with C203R mutations and the subject with the exon 2 deletion presented a classical BCM phenotype, with vision based solely

Investigative Ophthalmology and Visual Science, Vol. 53, No. 13 (December 2012): pg. 8006-8015. DOI.

on S cones and rods.[12,15] The two brothers with W177R mutations (JC_0355 and JC_0356) had an onset in the first decade with no history of nystagmus; both showed subsequent deterioration of visual acuity and color vision, macular pigment epithelial disturbance, and severe generalized cone dysfunction on ERG.[16] Both had good S-cone function with absent L/M cone function on psychophysical testing, though the data could not entirely exclude some residual L/M cone function in JC_0355.[16]

The remaining four subjects (JC_0347, JC_0564, JC_0118, KS_0577) had *OPN1LW* and *OPN1MW* mutations that fell into the newly discovered category involving intermixing of ancestral genes to produce L/M interchange mutations with deleterious combinations of nucleotides at normal polymorphic positions in exon 3.[7,8,10,13,19,24] All four of these subjects had a late-onset, progressive phenotype that was in stark contrast to that of the subjects with a C203R mutation or the exon 2 deletion (see Supplementary Material, http://www.iovs.org/content/53/13/8006/suppl/DC1). While the subjects with W177R mutations also had a progressive phenotype, it was earlier in onset than observed for the L/M interchange mutations and resulted in more complete loss of L/M cone function.

Reduced Retinal Thickness in Subjects with OPN1LW and OPN1MW Mutations

Topographical maps of retinal thickness show variable but significant macular thinning in individuals with all three classes of mutation (see Supplementary Material and Supplementary Fig. S1, http://www.iovs.org/content/53/13/8006/suppl/DC1). The average (±SD) central subfield (CSF) thickness (central 1 mm) for the 11 subjects examined here was 194 ± 34 μm, compared to an average (±SD) value for 60 normal subjects from our lab of 266 ± 19 μm; $P < 0.0001$, Mann-Whitney test.[25] The subjects with random point mutations had more normal CSF thickness (216 ± 20 μm) than the individuals with L/M interchange mutations (174 ± 28 μm); $P = 0.0381$, Mann-Whitney test. In addition, the retinal thinning in the subjects with L/M interchange mutations was more widespread (see

Investigative Ophthalmology and Visual Science, Vol. 53, No. 13 (December 2012): pg. 8006-8015. DOI.

Supplementary Material and Supplementary Fig. S1, http://www.iovs.org/content/53/13/8006/suppl/DC1).

To investigate the reduction in retinal thickness in more detail, we examined the thickness of the inner retina and the ONL+HFL from high-resolution horizontal cross sections (Fig. 1), and compared it to previously reported normative data.[14] Consistent with the topographical thickness analysis, we observed that subjects with random point mutations had more normal total retinal thickness than subjects in the other two genetic categories (Fig. 2A). However, subjects with random point mutations had thinning restricted to the ONL+HFL, while subjects with L/M interchange mutations (LVAVA, LIAVS, and LVVVA) or the exon 2 deletion showed parafoveal thinning of the inner retina in addition to reduced ONL+HFL thickness (Figs. 2B, B,22C).

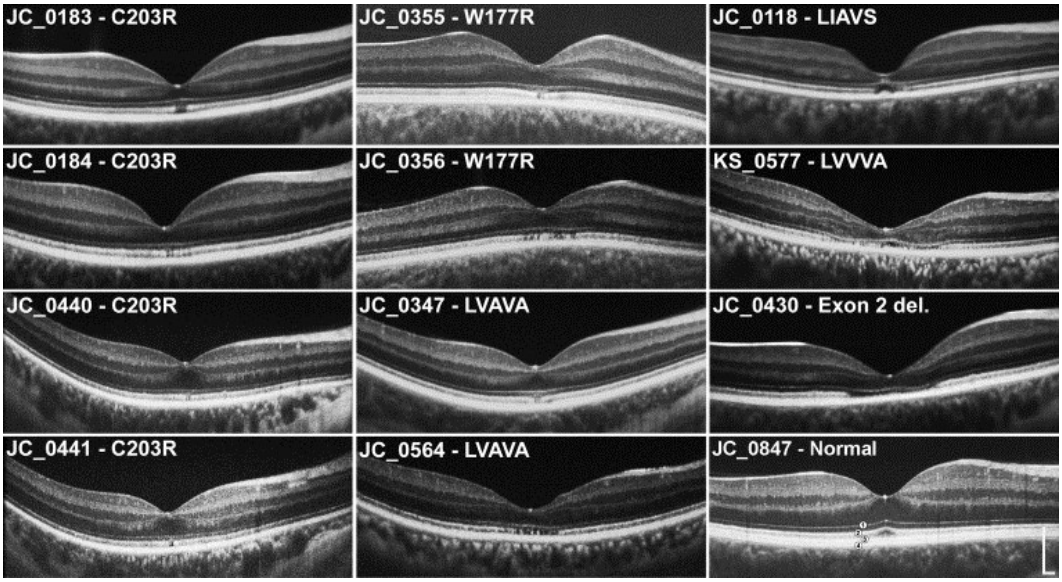

Figure 1. High-resolution SD-OCT images (horizontal line scans) through the fovea. Images are labeled with the subject ID and corresponding genotype. An image from a normal control (JC_0847) is shown for comparison (*lower right*). Four layers (labeled on the normal control scan) are associated with the hyperreflective photoreceptor complex, with layer 1 being attributed to the ELM and layer 2 to the ellipsoid portion of the inner segment (ISe). Layers 3 and 4 are thought to originate from different aspects of the RPE/photoreceptor interface and RPE, respectively.[34] Variable disruption of the ISe was observed across the 11 subjects. *Scale bar* is 200 μm.

Investigative Ophthalmology and Visual Science, Vol. 53, No. 13 (December 2012): pg. 8006-8015. DOI.

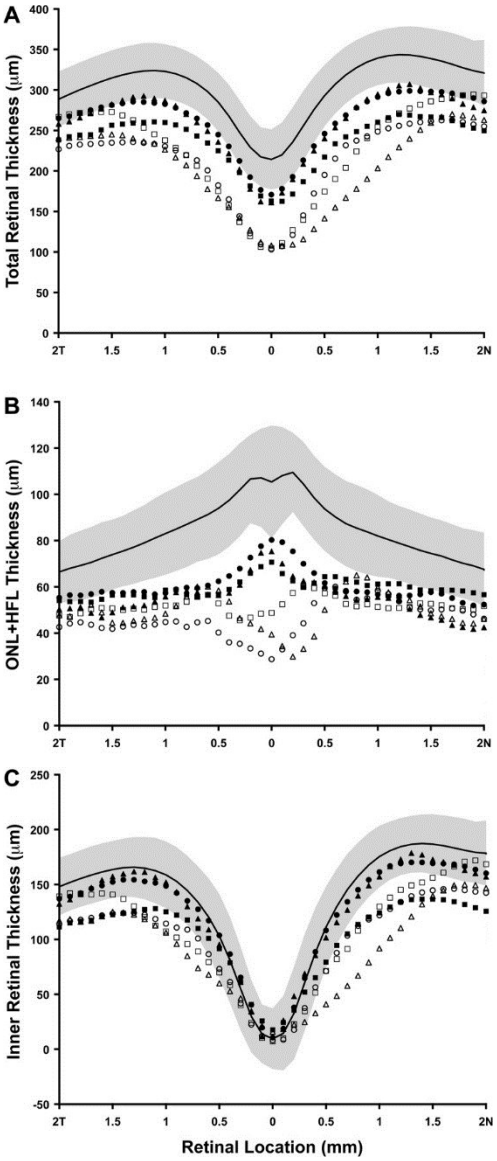

Figure 2. Retinal thickness analysis along the horizontal meridian. (**A**) Total retinal thickness, (**B**) ONL+HFL thickness, (**C**) inner retinal thickness. *Solid black line* represents mean values for 93 normal controls, with *shaded region* representing ±2 SD from the mean. *Filled circles* represent averaged data for the C203R subjects (JC_0183, JC_0184, JC_0440, JC_0441); *filled triangles* represent averaged data for the W177R subjects (JC_0355, JC_0356); *filled squares* represent averaged data for the LVAVA subjects (JC_0347, JC_0564); *open circles* represent data for the LIAVS subject (JC_0118); *open triangles* represent data for the LVVVA subject (KS_0577); and *open squares* represent data for the subject with the exon 2 deletion (JC_0430). All subjects showed significant retinal thinning (total and

ONL+HFL), with only the C203R and W177R subjects having normal inner retinal thickness.

Variable Appearance of Outer Photoreceptor Complex on SD-OCT in Subjects with OPN1LW and OPN1MW Mutations

In the normal retina, at least four hyperreflective bands comprise the outer photoreceptor complex (see JC_0847 in Fig. 1). The innermost peak of the outer photoreceptor complex is attributed to the ELM, while the second layer is now thought to derive from the ellipsoid portion of the inner segment (ISe).[34] The third layer is attributed to the RPE contact cylinder, and the fourth band is attributed to the RPE. As shown in Figure 1, we observed disruption of the ISe in all subjects; however, there were differences between the mutation classes that paralleled the differences in retinal thinning. Five of the six individuals with random point mutations (JC_0183, JC_0184, JC_0440, JC_0441, and JC_0355) had a focal disruption of the ISe near the foveal center. In contrast, subjects with L/M interchange mutations had generally greater disruption of the ISe: JC_0118 (LIAVS) and KS_0577 (LVVVA) had a large area of ISe loss (as did the subject with the exon 2 deletion, JC_0430), and JC_0564 (LVAVA) showed diffuse mottling of the ISe. However, these differences did not segregate perfectly with genotype category, as JC_0347 (LVAVA) had a well-defined focal lesion and JC_0356 (W177R) had diffuse mottling of the ISe.

In the six individuals with the focal ISe disruption, the boundaries of the disruption were marked using ImageJ[35]; the average (±SD) width was 99.2 ± 43.5 μm, consistent with previous estimates of the size of the S-cone free zone in humans.[36–38]

Disrupted Foveal Cone Mosaic in Subjects with OPN1LW and OPN1MW Mutations

Foveal montages created by stitching together multiple overlapping images are shown in Figure 3. Differences between the genotypic categories parallel those observed in the SD-OCT images.

Investigative Ophthalmology and Visual Science, Vol. 53, No. 13 (December 2012): pg. 8006-8015. DOI.

We observed a hyporeflective area at or near the foveal center in the six aforementioned subjects with a focal ISe disruption on SD-OCT, consistent with this small area lacking healthy, waveguiding cones. A sparse population of hyperreflective cones, presumably S cones, surrounded this hyporeflective area. The three subjects with a larger area of ISe loss on SD-OCT had irregular areas of hyperreflectivity in the foveal montages with minimal cone structure present, consistent with disruption of L, M, and S foveal cones in their macula. The remaining two subjects had more diffuse photoreceptor mosaic disruption across the foveal montage with only sporadic hyperreflective cones, in keeping with the irregularly disrupted ISe.

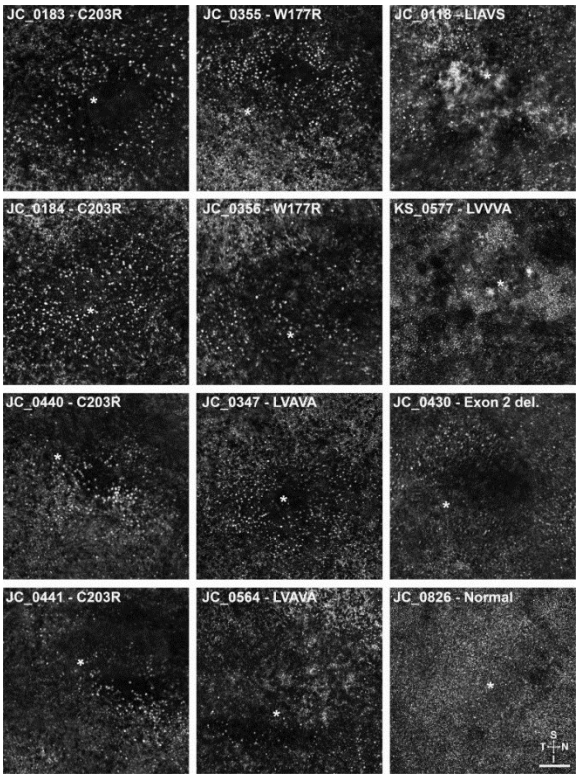

Figure 3. Variable disruption of the central photoreceptor mosaic. AOSLO montages of the photoreceptor mosaic are shown, created by stitching together multiple overlapping images. The location of the foveal pit is marked with an *asterisk*, and the orientation of the montages is provided at the *lower right* (S, superior; I, inferior; N, nasal; T, temporal). The location and extent of disruption visualized in the AOSLO montages was consistent with that seen on the SD-OCT images. *Scale bar* is 100 μm.

Investigative Ophthalmology and Visual Science, Vol. 53, No. 13 (December 2012): pg. 8006-8015. DOI.

Shown in Figure 4 are plots of the putative S cones observed in the foveal montages for the six subjects with a discrete disruption of the ISe, compared to a plot of similar data from Curcio et al.[38] While the analysis may not capture every S cone, it does provide a robust way to visualize the relative absence of reflective cones in a particular region. The size of the presumed S-cone free zone, determined by finding the largest circle that could be placed within the cone mosaic without encroaching on any cones, ranged from 50 to 120 μm, with an average of 72 μm for the six subjects. This is consistent with previous estimates of the size of the S-cone free zone,[36–38] providing further support that the focal ISe represents complete loss of L/M cone structure in the foveola. Interestingly, the center of the presumed S-cone free zone did not always align to the center of the foveal pit.

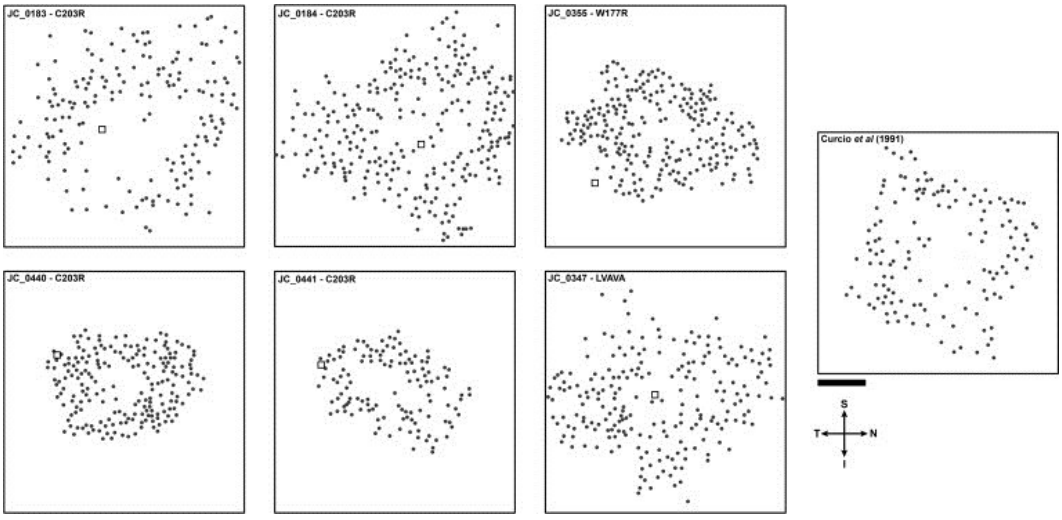

Figure 4. Visualizing the S-cone free zone. Shown are plots of putative S cones observed in the foveal montages for the six subjects with a discrete disruption of the ISe, compared to a plot of similar data from Curcio et al.[38] *Filled circles* are manually identified cones near the foveal center, identified by their bright, Gaussian reflective profile. *Open squares* represent the center of the foveal pit, and it is worth noting that the center of the presumed S-cone free zone does not always align to the center of the foveal pit. The analysis may not capture every S cone, and thus may not provide accurate estimates of S-cone density; however, it does provide a robust way to map the relative absence of reflective cones in a particular region. The size of the presumed S-cone free zone, determined by finding the largest circle that could be placed within the cone mosaic without encroaching on any cones, ranged from 50 to 120 μm, with an average of 72 μm for the six subjects. *Scale bar* is 100 μm.

Investigative Ophthalmology and Visual Science, Vol. 53, No. 13 (December 2012): pg. 8006-8015. DOI.

Residual Parafoveal L/M Cone Structure in Subjects with OPN1LW and OPN1MW Mutations

The parafoveal cone mosaic in subjects with *OPN1LW* and *OPN1MW* mutations is severely disrupted compared to normal (Fig. 5). However, there are important differences between the genetic categories. Between L/M interchange mutations and those with C203R mutations and W177R mutations, the severity of the losses was reversed compared to that in the foveal region. While the macula was generally thinner and the foveal region more disrupted for the interchange mutations as a group, their parafoveal cone numbers were better preserved in the parafovea (Fig. 6). The difference was largest at 2 mm from the fovea, the most eccentric location measured. We were not able to resolve the rod mosaic in all subjects, but measurements made outside the central area of ISe disruption (visible on OCT) showed rod density consistent with that measured previously in normals with the same technique (Fig. 7).[39]

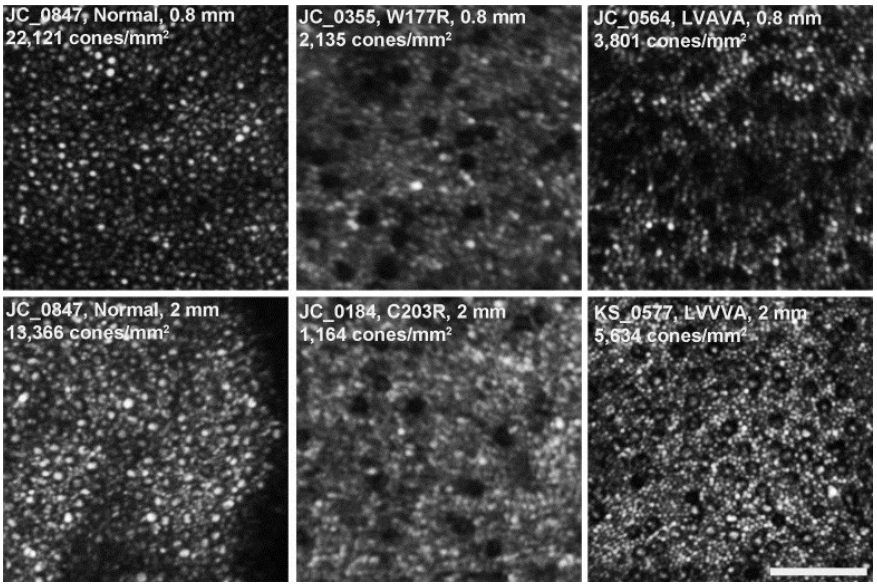

Figure 5. Disruption of the parafoveal photoreceptor mosaic. Eccentricity-matched images from a normal (*left*) compared to those from four of the mutations studied here (*middle* and *right*) are shown. The eccentricity of each image is given as the distance from the foveal center. In the normal images, cones are the larger structures and rods the smaller ones. In the subjects with *OPN1LW* and *OPN1MW* mutations, there are fewer cones compared to normal and the rods appear larger, but they still comprise a contiguous mosaic. *Scale bar* is 50 μm.

Investigative Ophthalmology and Visual Science, Vol. 53, No. 13 (December 2012): pg. 8006-8015. DOI.

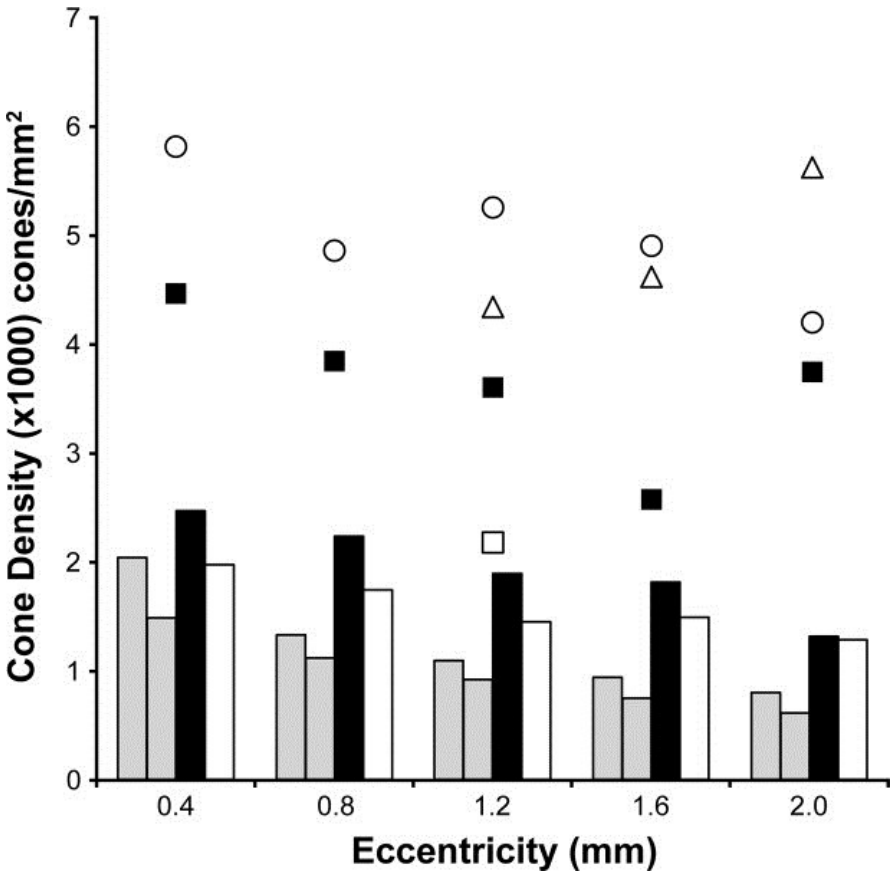

Figure 6. Genotype-dependent differences in retained cone structure. *Solid gray bars* represent the minimum and maximum S-cone density values reported in a previous histology study.[38] *Solid black bars* represent averaged data for the C203R subjects (JC_0183, JC_0184, JC_0440, JC_0441), while the *open bars* represent averaged data for the W177R subjects (JC_0355, JC_0356). *Filled squares* represent averaged data for the LVAVA subjects (JC_0347, JC_0564); *open circles* represent data for the LIAVS subject (JC_0118); *open triangles* represent data for the LVVVA subject (KS_0577); and the *open square* represents data for the subject with the exon 2 deletion (JC_0430).

Investigative Ophthalmology and Visual Science, Vol. 53, No. 13 (December 2012): pg. 8006-8015. DOI.

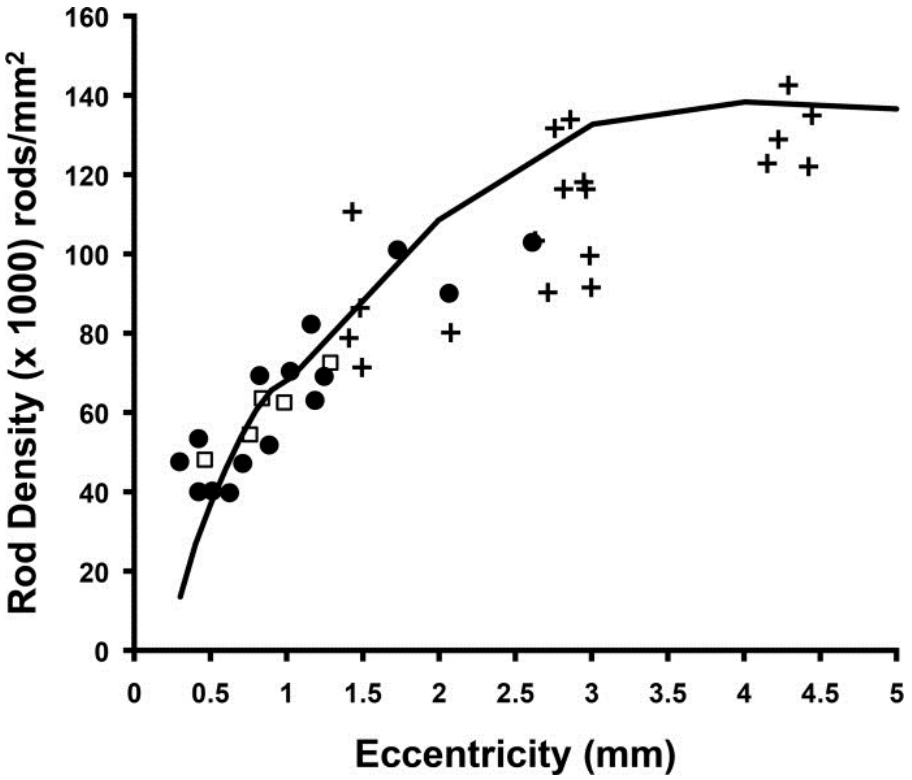

Figure 7. Parafoveal rod density in subjects with *OPN1LW* and *OPN1MW* mutations. It was not possible to visualize rods in all subjects or at systematic retinal locations, but in all areas assessed (eccentric to the central ISe disruption), we observed a contiguous rod mosaic of expected density. Subjects with C203R or W177R are plotted as *open squares*; subjects with L/M interchange mutations are plotted as *filled circles*; and the *crosses* represent normals measured using AOSLO from a previous study.[39] The *solid line* is the average rod density from a previous histology report.[40]

Assuming a starting cone density equal to that of an average normal,[40] the residual density for the subjects with the random point mutations was 8.5% of normal (SD = 3.0%), consistent with what would be expected if they had only S cones remaining.[37,38] In contrast, the subjects with L/M interchange mutations had residual densities that were on average 23% of normal (SD = 10.7%). Factoring in the expected population of S cones, we estimate that this corresponds to a loss of 86% of the L/M cones (SD = 9%). As normal cone density is highly variable, it is impossible to determine the exact degree of cone loss (or the degree of cone retention); however, it was clear that the retinas harboring C203R or W177R had very few, if any, residual L/M cones. Likewise, there was certainly residual L/M cone structure in

Investigative Ophthalmology and Visual Science, Vol. 53, No. 13 (December 2012): pg. 8006-8015. DOI.

subjects with L/M interchange mutations, consistent with the residual L/M cone function measured with the ERG in KS_0577, JC_0347, and JC_0564 (Kuchenbecker J, et al. *IOVS* 2012; 53:ARVO E-Abstract 6400). Structure/function agreement was also seen between the two subjects with the W77R mutation; JC_0355 had higher cone density and less retinal thinning than his brother (JC_0356), consistent with his slightly better vision in one eye and better L/M cone function on psychophysical testing.[16]

Discussion

Different Retinal Phenotypes in Subjects with OPN1LW and OPN1MW Mutations

While all subjects had disrupted photoreceptor mosaics and reduced retinal thickness, there were significant differences between the mutation classes. The imaging results provide a number of insights into the basis for the observed phenotypic differences between the mutation categories. In general, the six subjects with random missense mutations (C203R and W177R) had the healthiest-appearing retinas on SD-OCT. The small disruption of the ISe that was present was shown to correspond to the S-cone free zone,[36–38] with the focal loss of the ISe being the result of the absence of healthy L or M cones, S cones, or rods to provide structure at the foveal center.

In contrast to the C203R and W177R mutations, the L/M interchange mutations (four subjects) and exon 2 deletion (one subject) appear to be more disruptive to the overall foveal architecture. Only one of five of these subjects (JC_0347, LVAVA) had a small focal disruption of the ISe; the others had diffuse mottling of the ISe or a much larger absence of the ISe (extending into the parafovea). Compared to the subjects with the random point mutations, these subjects had greater retinal thinning that involved the inner retina as well as the ONL. This suggests that these L/M interchange mutations cause, or are associated with, degenerative changes that result in damage to neighboring cells (S cones and rods) in addition to those expressing mutant L/M opsin.

Investigative Ophthalmology and Visual Science, Vol. 53, No. 13 (December 2012): pg. 8006-8015. DOI.

The specificity of the photoreceptor damage to the macular region in the subjects with L/M interchange mutations is striking when images of the fovea are compared to more peripheral ones. Retinoid by-products of the visual cycle and all-trans-retinal (atRAL) are particularly toxic.[41] It is possible that the cones expressing the L/M interchange mutants remain viable through young adulthood but are defective in their ability to participate normally in the visual cycle. This could lead to a buildup of atRAL or other toxic retinoids, affecting not only the cones expressing the mutant opsin, but also parafoveal S cones and rods. If these toxic by-products are concentrated in the fovea where the cone density is 20 times higher than in the peripheral retina,[40] it could explain why the collateral damage is higher at the central retina compared to more eccentric locations (Fig. 1).

Implications for Restoration of Visual Function in Subjects with OPN1LW and OPN1MW Mutations

Advances in gene therapy have generated a great deal of excitement regarding the restoration of cone function in a variety of retinal diseases.[42–48] While subjects with L/M interchange mutations had the greatest degree of residual parafoveal L/M cone structure, the presence of macular atrophy and inner retinal thinning in most of these subjects would limit the therapeutic opportunity in these individuals at later stages of the disease. However, strategies may be developed to slow the degenerative effects of these mutations. In contrast, the subjects with C203R or W177R mutations generally had more preserved retinal lamination, but adaptive optics imaging revealed no evidence for retained L/M cone structure. It is unclear whether any cone cell bodies remain, though given that rods appear to have expanded to fill in the space occupied by the cones, this would imply degeneration of at least the inner and outer segments.

We did not examine subjects with deletions involving the locus control region (LCR), so it remains to be seen how complete absence of L/M opsin affects cone photoreceptor integrity compared to the expression of mutant opsin. Furthermore, we are unable to say if there are structural differences between individuals harboring different L/M interchange mutations. Previous evidence showed that an individual

Investigative Ophthalmology and Visual Science, Vol. 53, No. 13 (December 2012): pg. 8006-8015. DOI.

with the LIAVA mutant expressed by one of the two genes in the L/M array had random, non-waveguiding cells throughout the cone mosaic, normal ISe integrity, normal inner retinal thickness, and no change in cone structure measured over a span of 8 years.[8,18] This suggests that the LIAVA mutant may not result in the progressive loss of L/M cones (or does so on a much slower time scale), and it will be important to longitudinally assess the progressive nature of the various L/M interchange mutations to better determine the therapeutic potential in these individuals.

In addition to using the imaging tools described here to prioritize potential subjects most suitable for intervention, by characterizing the degree of residual cone structure in subjects with *OPN1LW* and *OPN1MW* mutations, it will be valuable to employ the same techniques when evaluating the safety and efficacy of any future therapeutic intervention. Such an approach has already been demonstrated in patients with retinitis pigmentosa receiving ciliary neurotrophic factor,[49] where preservation of cone structure was observed in the absence of a significant functional improvement in vision. It is entirely plausible that structural recovery or preservation precedes functional changes; however, this will remain unclear until high-resolution imaging metrics become a routine part of the outcome measures used in clinical trials.

Acknowledgments

The authors thank Pooja Godara, Zach Harvey, Jennifer Norris, Jungtae Rha, Netta Smith, and Phyllis Summerfelt for assistance with the study.

Footnotes

Supported by NEI Grants P30 EY001931 (JC), R01 EY017607 (JC), T32 EY014537 (AMD), UL1 RR031973 (KES, JC), R01 EY014375 (DRW), P30 EY001319 (DRW), P30 EY001730 (MN, JN), R01 EY009303 (MN), and R01 EY009620 (JN); supported by grants from the Gene and Ruth Posner Foundation (JC), Foundation Fighting Blindness (JC, MM), The E. Matilda Ziegler Foundation for the Blind (JC), the RD & Linda Peters Foundation (JC), unrestricted departmental grants from

Research to Prevent Blindness (Medical College of Wisconsin, University of Washington, University of Illinois-Chicago), the Juvenile Diabetes Research Foundation (8-2002-130), Fight for Sight UK (AJH, MM), Moorfields Eye Hospital Special Trustees (AJH, MM), and the National Institute for Health Research Biomedical Research Centre at Moorfields Eye Hospital NHS Foundation Trust and UCL Institute of Ophthalmology (AJH, ATM, MM); and supported in part by Grant No. 3000003241 from the Chief Scientist Office of the Ministry of Health, Israel, and the Yedidut Research Grant (DS, EB). J. Carroll and A. Dubra are recipients of Career Development Awards from Research to Prevent Blindness. A. Dubra is the recipient of a Career Award at the Scientific Interface from the Burroughs Wellcome Fund. M. Michaelides is a recipient of a Career Development Award from the Foundation Fighting Blindness. This investigation was conducted in part in a facility constructed with support from the Research Facilities Improvement Program; Grant C06 RR016511 from the National Center for Research Resources, National Institutes of Health. DRW holds patents on adaptive optics imaging.

Disclosure: **J. Carroll**, Imagine Eyes, Inc. (S); **A. Dubra**, None; **J.C. Gardner**, None; **L. Mizrahi-Meissonnier**, None; **R.F. Cooper**, None; **A.M. Dubis**, None; **R. Nordgren**, None; **M. Genead**, None; **T.B. Connor Jr**, None; **K.E. Stepien**, None; **D. Sharon**, None; **D.M. Hunt**, None; **E. Banin**, None; **A.J. Hardcastle**, None; **A.T. Moore**, None; **D.R. Williams**, Canon (F), Polgenix (F), Pfizer (C), P, GlaxoSmithKline (C), P, Pfizer (R); **G. Fishman**, None; **J. Neitz**, None; **M. Neitz**, None; **M. Michaelides**, None

References

1. Nathans J, Davenport CM, Maumenee IH, et al. Molecular genetics of human blue cone monochromacy. *Science*. 1989;245:831–838
2. Winderickx J, Sanocki E, Lindsey DT, et al. Defective colour vision associated with a missense mutation in the human green visual pigment gene. *Nat Genet*. 1992;1:251–256
3. Nathans J, Maumenee IA, Zrenner E, et al. Genetic heterogeneity among blue-cone monochromats. *Am J Hum Genet*. 1993;53:987–1000
4. Ayyagari R, Kakuk LE, Toda Y, et al. Blue cone monochromacy: macular degeneration in individuals with cone specific gene loss. In: Hollyfield

JG, RE Anderson, LaVail MM, editors. eds *Retinal Degenerative Diseases and Experimental Therapy*. New York: Kluwer Academic/Plenum Publishers; 1999

5. Jagla WM, Jägle H, Hayashi T, et al. The molecular basis of dichromatic color vision in males with multiple red and green visual pigment genes. *Hum Mol Genet*. 2002;11:23–32
6. Kellner U, Wissinger B, Tippmann S, et al. Blue cone monochromatism: clinical findings in patients with mutations in the red/green opsin gene cluster. *Graefes Arch Clin Exp Ophthalmol*. 2004;242:729–735
7. Neitz M, Carroll J, Renner A, et al. Variety of genotypes in males diagnosed as dichromatic on a conventional clinical anomaloscope. *Vis Neurosci*. 2004;21:205–216
8. Carroll J, Neitz M, Hofer H, et al. Functional photoreceptor loss revealed with adaptive optics: an alternate cause for color blindness. *Proc Natl Acad Sci U S A*. 2004;101:8461–8466
9. Young TL, Deeb SS, Ronan SM, et al. X-linked high myopia associated with cone dysfunction. *Arch Ophthalmol*. 2004;122:897–908
10. Crognale MA, Fry M, Highsmith J, et al. Characterization of a novel form of X-linked incomplete achromatopsia. *Vis Neurosci*. 2004;21:197–203
11. Michaelides M, Johnson S, Bradshaw K, et al. X-linked cone dysfunction syndrome with myopia and protanopia. *Ophthalmology*. 2005;112:1448–1454
12. Michaelides M, Johnson S, Simunovic MP, et al. Blue cone monochromatism: a phenotype and genotype assessment with evidence of progressive loss of cone function in older individuals. *Eye*. 2005;19:2–10
13. Mizrahi-Meissonnier L, Merin S, Banin E, Sharon D. Variable retinal phenotypes caused by mutations in the X-linked photopigment gene array. *Invest Ophthalmol Vis Sci*. 2010;51:3884–3892
14. Carroll J, Baraas RC, Wagner-Schuman M, et al. Cone photoreceptor mosaic disruption associated with Cys203Arg mutation in the M-cone opsin. *Proc Natl Acad Sci U S A*. 2009;106:20948–20953
15. Gardner JC, Michaelides M, Holder GE, et al. Blue cone monochromacy: causative mutations and associated phenotypes. *Mol Vis*. 2009;15:876–884
16. Gardner JC, Webb TR, Kanuga N, et al. X-linked cone dystrophy caused by mutation of the red and green cone opsins. *Am J Hum Genet*. 2010;87:26–39
17. Wagner-Schuman M, Neitz J, Rha J, et al. Color-deficient cone mosaics associated with Xq28 opsin mutations: a stop codon versus gene deletions. *Vision Res*. 2010;50:2396–2402

18. Rha J, Dubis AM, Wagner-Schuman M, et al. Spectral domain optical coherence tomography and adaptive optics: imaging photoreceptor layer morphology to interpret preclinical phenotypes. *Adv Exp Med Biol*. 2010;664:309–316
19. Neitz J, Neitz M. The genetics of normal and defective color vision. *Vision Res*. 2011;51:633–651
20. Carroll J, Neitz M, Neitz J. Estimates of L:M cone ratio from ERG flicker photometry and genetics. *J Vision*. 2002;2:531–542
21. Hofer H, Carroll J, Neitz J, et al. Organization of the human trichromatic cone mosaic. *J Neurosci*. 2005;25:9669–9679
22. Jacobson SG, Aleman TS, Cideciyan AV, et al. Identifying photoreceptors in blind eyes caused by RPE65 mutations: prerequisite for human gene therapy success. *Proc Natl Acad Sci U S A*. 2005;102:6177–6182
23. Ladekjaer-Mikkelsen A-S, Rosenberg T, Jørgensen AL. A new mechanism in blue cone monochromatism. *Hum Genet*. 1996;98:403–408
24. Ueyama H, Muraki-Oda S, Yamade S, et al. Unique haplotype in exon 3 of cone opsin mRNA affects splicing of its precursor, leading to congenital color vision defect. *Biochem Biophys Res Commun*. 2012;424:152–157
25. Wagner-Schuman M, Dubis AM, Nordgren RN, et al. Race- and sex-related differences in retinal thickness and foveal pit morphology. *Invest Ophthalmol Vis Sci*. 2010;52:625–634
26. Tanna H, Dubis AM, Ayub N, et al. Retinal imaging using commercial broadband optical coherence tomography. *Br J Ophthalmol*. 2010;94:372–376
27. Dubra A, Sulai Y. Reflective afocal broadband adaptive optics scanning ophthalmoscope. *Biomed Opt Express*. 2011;2:1757–1768
28. Cooper RF, Dubis AM, Pavaskar A, et al. Spatial and temporal variation of rod photoreceptor reflectance in the human retina. *Biomed Opt Express*. 2011;2:2577–2589
29. Gray DC, Merigan W, Wolfing JI, et al. In vivo fluorescence imaging of primate retinal ganglion cells and retinal pigment epithelial cells. *Opt Express*. 2006;14:7144–7158
30. ANSI American National Standard for Safe Use of Lasers (ANSI Z136.1). *ANSI Z1361-2007*. The Laser Institute of America; 2007
31. Delori FC, Webb RH, Sliney DH. Institute ANS. Maximum permissible exposures for ocular safety (ANSI 2000), with emphasis on ophthalmic devices. *J Opt Soc Am A*. 2007;24:1250–1265
32. Dubra A, Harvey Z. Registration of 2D images from fast scanning ophthalmic instruments. *The 4th International Workshop on Biomedical Image Registration*. Lübeck, Germany; 2010

Investigative Ophthalmology and Visual Science, Vol. 53, No. 13 (December 2012): pg. 8006-8015. DOI.

33. Garrioch R, Langlo C, Dubis AM, et al. Repeatability of in vivo parafoveal cone density and spacing measurements. *Optom Vis Sci*. 2012;89:632–643
34. Spaide RF, Curcio CA. Anatomical correlates to the bands seen in the outer retina by optical coherence tomography: literature review and model. *Retina*. 2011;31:1609–1619
35. Abramoff MD, Magelhaes PJ, Ram SJ. Image processing with ImageJ. *Biophotonics Int*. 2004;11:36–42
36. Williams DR, MacLeod DIA, Hayhoe MM. Punctate sensitivity of the blue-sensitive mechanism. *Vision Res*. 1981;21:1357–1375
37. Ahnelt PK, Kolb H, Pflug R. Identification of a subtype of cone photoreceptor, likely to be blue sensitive, in the human retina. *J Comp Neurol*. 1987;255:18–34
38. Curcio CA, Allen KA, Sloan KR, et al. Distribution and morphology of human cone photoreceptors stained with anti-blue opsin. *J Comp Neurol*. 1991;312:610–624
39. Dubra A, Sulai Y, Norris JL, et al. Non-invasive imaging of the human rod photoreceptor mosaic using a confocal adaptive optics scanning ophthalmoscope. *Biomed Opt Express*. 2011;2:1864–1876
40. Curcio CA, Sloan KR, Kalina RE, Hendrickson AE. Human photoreceptor topography. *J Comp Neurol*. 1990;292:497–523
41. Chen Y, Okano K, Maeda T, et al. Mechanism of all-trans-retinal toxicity with implications for stargardt disease and age-related macular degeneration. *J Biol Chem*. 2012;287:5059–5069
42. Alexander JJ, Umino Y, Everhart D, et al. Restoration of cone vision in a mouse model of achromatopsia. *Nat Med*. 2007;13:685–687
43. Maguire AM, Simonelli F, Pierce EA, et al. Safety and efficacy of gene transfer for Leber's congenital amaurosis. *N Engl J Med*. 2008;358:2240–2248
44. Bainbridge JW, Smith AJ, Barker SS, et al. Effect of gene therapy on visual function in Leber's congenital amaurosis. *N Engl J Med*. 2008;358:2231–2239
45. Cideciyan AV, Aleman TS, Boye SL, et al. Human gene therapy for RPE65 isomerase deficiency activates the retinoid cycle of vision but with slow rod kinetics. *Proc Nat Acad Sci U S A*. 2008;105:15112–15117
46. Mancuso K, Hauswirth WW, Li Q, et al. Gene therapy for red-green colour blindness in adult primates. *Nature*. 2009;461:784–787
47. Komáromy A, Alexander JJ, Rowlan JS, et al. Gene therapy rescues cone function in congenital achromatopsia. *Hum Mol Genet*. 2010;19:2581–2593
48. Carvalho LS, Xu J, Pearson R, et al. Long-term and age-dependent restoration of visual function in a mouse model of CNGB3-associated

achromatopsia following gene therapy. *Hum Mol Genet*. 2011;20:3161–3175

49. Talcott KE, Ratnam K, Sundquist S, et al. Longitudinal study of cone photoreceptors during retinal degeneration and in response to ciliary neurotrophic factor treatment. *Invest Ophthalmol Vis Sci*. 2011;52:2219–2226